Published in final edited form as:

ACS Appl Mater Interfaces. 2017 July 12; 9(27): 22893–22901. doi:10.1021/acsami.7b03965.

Aluminum (oxy)hydroxide nanosticks synthesized in bicontinuous reverse microemulsion have potent vaccine adjuvant activity

Xu Li[1], **Stephanie Hufnagel**[1], **Haiyue Xu**[1], **Solange A. Valdes**[1], **Sachin G. Thakkar**[1], **Zhengrong Cui**[1,2,*], and **Hugo Celio**[3]

[1]The University of Texas at Austin, College of Pharmacy, Division of Molecular Pharmaceutics and Drug Delivery, Austin, Texas, U.S.A

[2]Inner Mongolia Medical University, Inner Mongolia Key Laboratory of Molecular Biology, Hohhot, Inner Mongolia, China

[3]The University of Texas at Austin, Texas Materials Institute, Austin, Texas, U.S.A

Abstract

Insoluble aluminum salts such as aluminum (oxy)hydroxide are commonly used vaccine adjuvants. Recently, there is evidence suggesting that the adjuvant activity of aluminum salt-based materials is tightly related to their physico-chemical properties, including nanometer-scale size, shape with long aspect ratio, and low degree of crystallinity. Herein, for the first time, the bicontinuous reverse microemulsion (RM) technique was utilized to synthesize stick-like monodisperse aluminum (oxy)hydroxide nanoparticles with a long aspect ratio of ~10, length of ~80 nm and low degree of crystallinity (denoted as Al-nanosticks). Moreover, the relationship between the physico-chemical properties of Al-nanosticks and the bicontinuous RM was discussed. Compared to the commercial Alhydrogel®, which contains micrometer-scale aluminum oxyhydroxide particular aggregates with a moderate degree of crystallinity, the Al-nanosticks are more effective in adsorbing and delivering antigens (e.g. ovalbumin, OVA) into antigen-presenting cells, activating inflammasomes, and potentiating OVA-specific antibody responses in a mouse model. It is concluded that the aluminum (oxy)hydroxide nanosticks synthesized in the bicontinuous RM are promising new aluminum salt-based vaccine adjuvants.

Keywords

aluminum salt-based materials; nanoparticle synthesis; physico-chemical properties; antigen delivery; immune responses

[*]Author of correspondence Tel: (512) 495-4758, Zhengrong.cui@austin.utexas.edu.

Supporting Information

TEM images of the aluminum hydroxide particular aggregates prepared by the ‘co-precipitation’ method and the commercial Alhydrogel® (2%, w/v); comparison of the XRD pattern of Al-nanosticks with those of standard boehmite, bayerite and gibbsite; detection of the residual NP-5 content in Al-nanosticks.

Introduction

Adjuvants are often needed in new generation vaccines to amplify, guide, and/or accelerate the resultant immune responses.[1–3] Insoluble aluminum salt-based particular materials (e.g. aluminum (oxy)hydroxide or (hydroxy)phosphate), known as 'Alum', are commonly used as adjuvants in a variety of vaccines.[4–8] However, traditional Alum adjuvants only moderately potentiate antigen-specific antibody responses.[9–10] Recent evidence shows that the activity of aluminum salt-based adjuvants can be significantly improved by rationally modifying their physical and/or chemical properties.[11] For instance, traditional Alum adjuvants are aluminum salt-based particular aggregates with irregular shape and micrometer-scale size.[12–13] We previously showed that aluminum hydroxide and aluminum phosphate nanoparticles have significantly more potent adjuvant activity than their corresponding microparticles, likely related to the nanoparticles' ability to increase the uptake of the antigens adsorbed on them by antigen-presenting cells (APCs) and to activate inflammasomes.[14–16] Such size-dependent enhancement of the adjuvant effect of aluminum salt-based materials has also been reported by others.[4, 17] For example, Wang and colleagues developed lipid-enveloped aluminum hydroxide nanoparticles with stronger adjuvant activity than aluminum hydroxide microparticles.[17] In addition to the particle size, other properties of aluminum salt-based materials can influence their adjuvant activity as well. For instance, Sun et al. have prepared a library of nanorod-like aluminum oxyhydroxide (AlOOH) particles and found that such particles containing more hydroxyl groups (i.e. with lower degree of crystallinity) are more effective in activating NALP3 inflammasomes.[13] Moreover, when compared to nanoplate-like and nanopolyhedron-like aluminum oxyhydroxide particles, the nanorod-like particles with long aspect ratios are also more effective in activating NLRP3 inflammasomes.[13] Taken together, data from these studies demonstrate that the physico-chemical properties (e.g. size, shape, and crystallinity) of aluminum salt-based materials significantly affect their adjuvant activities.

The reverse microemulsion (RM) technique has undergone rapid development in the past several decades, especially for its application in the design and manipulation of nanoparticulate materials.[18–21] In general, the formation of nanoparticles in RM is based on the 'template' concept, i.e. the shape of particles should repeat the shape of the inner water phase of the RM in which they are synthesized.[21–23] As a result, RM systems with diverse non-spherically shaped inner water phases have been developed, characterized, and used to prepare nanoparticles with unique shapes. [21, 24] For instance, bicontinuous RM is a type of RM with a channel-like (also expressed as 'interconnected cylinder-like') inner water phase, and it has been used to prepare metallic salt-based or pure metallic nanoparticles with long aspect ratios, i.e. in the form of rods, filaments, wires, pearl necklaces, etc.[25–31] Although the synthesis of aluminum salt-based material in a bicontinuous RM system has not been reported yet, it is expected that the channel-like water phase can modulate the formation of such material to obtain particles with sizes in nanometer-scale and shapes with long aspect ratios. These characteristics are important factors in determining the relative adjuvant activity of the aluminum salt-based materials as mentioned above.[13–17]

In the present study, a bicontinuous RM system prepared with water, polyoxyethylene (5) nonylphenylether (NP-5) and cyclohexane was used to synthesize a type of stick-like

monodisperse aluminum (oxy)hydroxide nanoparticles with low degree of crystallinity (denoted as Al-nanosticks). The physico-chemical properties of such Al-nanosticks were characterized and their relationship with the properties of bicontinuous RM was discussed. Thereafter, the ability of Al-nanosticks to deliver antigen into APCs and activate inflammasomes were investigated. Finally, the adjuvant activity of the Al-nanosticks was evaluated in a mouse model and compared to that of Alhydrogel® (2%, w/v) (denoted as Alhydrogel), the international standard preparation of aluminum (oxy)hydroxide gels.

Materials and Methods

Reagents

Aluminum chloride ($AlCl_3$) hexahydrate, aluminum hydroxide hydrate (aluminum hydroxide powder), sodium hydroxide, ammonium hydroxide solution, ovalbumin (OVA), sodium bicarbonate, sodium carbonate, phosphate-buffered saline (PBS), horse serum, Lugol's solution (Iodine/Potassium iodide solution), polyoxyethylene (5) nonylphenylether (NP-5), paraformaldehyde and 3-(4,5-dimethylthiazol-2-yl)-2,5-diphenyltetrazolium bromide (MTT) reagent were from Sigma-Aldrich (St. Louis, MO). Alhydrogel, phorbol 12-myristate 13-acetate (PMA), lipopolysaccharide (LPS), and monosodium urate (MSU) crystal were from InvivoGen (San Diego, CA). Cyclohexane, ethanol, fluorescein conjugated ovalbumin (FITC-OVA), 4',6-diamidino-2-phenylindole dihydrochloride (DAPI) and Pierce™ BCA protein assay kit were from Thermo Fisher Scientific Co. (Pittsburgh, PA). Horseradish peroxidase-labeled goat anti-mouse immunoglobulins (IgG, IgG1, and IgG2a) were from Southern Biotechnology Associates, Inc. (Birmingham, AL). Human IL-1β enzyme-linked immunosorbent assay (ELISA) kit was from R&D Systems (Minneapolis, MN).

Cells and Animals

Fetal bovine serum (FBS), DMEM and RPMI-1640 cell culture media, and antibiotics (penicillin-streptomycin) were from Invitrogen (Carlsbad, CA). Murine J774A.1 macrophages and human THP-1 cells were from the American Type Culture Collection (Manassas, VA). J774A.1 cells were grown at 37°C with 5% CO_2 in DMEM supplemented with 10% FBS (v/v), 100 U/mL-100 μg/mL penicillin-streptomycin. THP-1 cells were grown at 37 °C with 5% CO_2 in RPMI-1640 supplemented with 10% FBS (v/v), 100 U/mL-100 μg/mL penicillin-streptomycin, and 50 μM β-mercaptoethanol.

Female BALB/c mice, 6–8 weeks of age, were from Charles River Laboratories, Inc. (Wilmington, MA). Animal studies were performed in accordance with the United States National Research Council Guide for the Care and Use of Laboratory Animals. Animal protocol was approved by the Institutional Animal Care and Use Committee at The University of Texas at Austin.

Synthesis of Al-nanosticks in bicontinuous RM

To prepare Al-nanosticks, we used the RM system prepared with a water/NP-5 molar ratio of ~16, which was a bicontinuous type of RM with a channel-like water phase.[32–33] An aqueous solution of 0.1 M $AlCl_3$ or 0.6 M ammonium hydroxide (0.4 mL for each) was

added into 8 mL of the mixture of NP-5/cyclohexane (v/v, 7.5/92.5), followed by water bath sonication until the system became transparent. Afterwards, such two types of RM were mixed with each other to initiate the reaction between Al^{3+} and OH^{-}. After overnight reaction (~16 h) at room temperature (~22 °C), the mixed RM was transferred into abundant ethanol, and the resultant mixture was centrifuged at 13 000 × g for 40 min. The precipitate was washed twice with ethanol and suspended in water. Thereafter, the suspension was passed through a 0.45 μm Nylon filter (Thermo Fisher Scientific) and stored at 4 °C. For X-ray powder diffraction (XRD), thermogravimetric analysis (TGA), and X-ray photoelectron spectroscopy (XPS), after washing with ethanol, the products suspended in ethanol were further dialyzed against ethanol using a dialysis membrane (MWCO, ~12 KDa, Spectrum Laboratories, Inc., Rancho Dominguez, CA). Dialysis was repeated against water and the particles were then lyophilized into a dry powder using a FreeZone freeze dry system (Labconco, Kansas City, MO). The content of residual NP-5 surfactant in the purified Al-nanostick preparation was estimated using Lugol's solution,[34] as the NP-5 has a polyoxyethylene moiety.

As a control, aluminum hydroxide particles were also prepared using the 'co-precipitation' method.[35] Briefly, 0.6 M ammonia solution was added directly into the solution of 0.1 M $AlCl_3$ (0.4 mL for each) under magnetic stirring. After overnight reaction at room temperature, precipitates were collected by centrifugation at 13 000 × g for 20 min and washed twice using water. The final product was either stored in water or lyophilized into a dry powder.

Characterization of the physical properties of the Al-nanosticks

The morphology of the Al-nanosticks was observed using a Tecnai transmission electron microscope (TEM, FEI, Hillsboro, OR) operated with high tension of 80 kV. Specimens were prepared by placing a small volume (~5 μL) of the aqueous suspension of Al-nanosticks onto a carbon film-coated copper grid (Electron Microscopy Sciences, Hatfield, PA). The suspension was allowed to air-dry before observation.

XRD analysis of the Al-nanosticks in powder was performed using an R-Axis Spider with a Cu sealed tube source and a large, image plate detector (Rigaku, The Woodlands, TX). Aluminum hydroxide particles prepared by the 'co-precipitation' method, commercial Alhydrogel, and commercial aluminum hydroxide powder were also treated by lyophilization and then characterized for comparison. All XRD patterns were collected with a step size of 0.01 and counting time of 1 s per step over a 2θ range of 10 to 80.

TGA of the Al-nanosticks in powder was carried out with a Thermogravimetric Analyzer, Model TGA/DSC (Mettler Toledo, Columbus, OH). All of the samples were heated from 30 to 1000 °C at a rate of 10 °C/min in air. Again, aluminum hydroxide particles prepared by the 'co-precipitation' method, Alhydrogel, and commercial aluminum hydroxide powder were treated by lyophilization and analyzed for comparison.

XPS characterization of Al-nanosticks was carried out using an X-ray Photoelectron Spectrometer (Kratos Axis Ultra DLD, Manchester, U.K.), utilizing a monochromated Al-K-alpha X-ray source (hv = 1486.5 eV), X-ray power at 120 Watts, hybrid optics (employing

a magnetic and electrostatic lens simultaneously), and a multi-channel plate detector coupled to a hemispherical photoelectron kinetic analyzer. The base pressure in the analysis chamber was typically 6×10^{-9} Torr. Powder samples were pressed on carbon tape and spectra were collected with a passing energy of 20 eV and scanned at 0.1 eV per step. To correct the charge surplus shifting, peak positions of the samples were calibrated with respect to the C 1s region of adventitious hydrocarbons adsorbed on the samples, i.e., C 1s, at 284.8 eV. The Casa XPS Analysis Software (Casa Software Ltd., Teignmouth, UK) was used for peak fitting analysis, and the stoichiometric ratios were determined from corrected peak areas by employing the Kratos sensitivity factors for each element of interest.

The concentration of aluminum in each sample was measured using a Varian 710-ES inductively coupled plasma-optical emission spectrometer (ICP-OES, Agilent Technologies, Santa Clara, CA) and expressed as the concentration of Al^{3+}.

Characterizations of OVA-adsorbed Al-nanosticks

The adsorption of OVA onto Al-nanosticks was carried out by directly mixing an OVA solution with an aqueous suspension of Al-nanosticks. A solution containing a fixed amount of OVA was mixed with an equal volume of a suspension of Al-nanosticks with various concentrations of aluminum to adjust the Al^{3+}/OVA weight ratios from 0.025/1 to 5/1. After mixing for 15 min, the mixture was centrifuged at 15 000 × g for 10 min, and the amount of OVA in the supernatant was determined using a Pierce™ BCA protein assay kit. The percent of OVA adsorbed was calculated accordingly. The hydrodynamic sizes and zeta potentials of the OVA-adsorbed Al-nanosticks were also determined using a Malvern Zetasizer Nano ZS (Westborough, MA). For comparison, the adsorption of OVA to Alhydrogel, and the sizes and zeta potentials of the resultant OVA-adsorbed Alhydrogel were also determined. In these experiments, triplicate samples were tested for each group. Finally, the morphology of the OVA-adsorbed Al-nanosticks prepared with an Al^{3+}/OVA weight ratio of 5/1 was observed using TEM. The sample was negatively stained using uranyl acetate before observation.

Uptake of OVA adsorbed on Al-nanosticks by macrophages in culture

Murine J774.1A macrophages were seeded in Nunc™ glass bottom dishes (Thermo Fisher Scientific) with a density of 2×10^6 per well. After overnight incubation, free FITC-OVA or FITC-OVA adsorbed on Al-nanosticks or Alhydrogel (Al^{3+}/OVA weight ratio, 5/1) was added into the culture medium (final Al^{3+} concentration of 10 μg/mL). After six additional hours of incubation, cells were washed with cold PBS three times, and then fixed with 4% paraformaldehyde for 15 min at room temperature. Cells were washed with PBS twice, incubated with a PBS solution containing DAPI for 15 min, washed with PBS twice again, and then examined using a Leica SP5 AOBS WLL confocal microscope (Leica, Buffalo Grove, IL).

IL-1β secretion by THP-1 stimulated with Al-nanosticks

THP-1 cells were seeded into 96-well plates at a density of 3×10^4 per well. PMA (1 μg/mL) was added into the culture medium and kept for 16 h to allow the differentiation of the monocytes into macrophages. Thereafter, the culture medium was replaced by fresh serum-free medium without PMA, and the cells were incubated with the Al-nanosticks or

commercial Alhydrogel (Al^{3+} concentration, 50 μg/mL) in the presence or absence of 10 ng/mL LPS (n = 6).[15] A group of cells treated with MSU plus LPS was used as a positive control. After 6 h of incubation, IL-1β concentration in the culture medium was determined using a R&D Systems IL-1β ELISA kit following the manufacturers' instructions. The endotoxin levels in the Al-nanosticks or Alhydrogel preparations diluted in cell culture medium to an Al^{3+} concentration of 50 μg/mL were measured using a ToxinSensor™ Chromogenic Limulus Amebocyte Lysate Endotoxin Assay Kit from GenScript (Piscataway, NJ) and found to be 0.05 ± 0.01 EU/ml and 0.03 ± 0.01 EU/ml, respectively, which are not different from the endotoxin level in the cell culture medium (i.e. 0.04 ± 0.01 EU/ml; p = 0.32 vs. Al-nanosticks, p = 0.29 vs. Alhydrogel, n = 3).

Mouse immunization studies and histological examination

Female BALB/c mice (6–8 weeks, n = 5) were subcutaneously (s.c.) injected with free OVA, OVA-adsorbed Al-nanosticks or OVA-adsorbed Alhydrogel once every two weeks for a total of three injections. The dose of the OVA was 5 μg per mouse per injection, and the Al^{3+}/OVA weight ratio was 5/1. Thirty-one days after the last injection, OVA-specific serum total IgG, IgG1, and IgG2a levels were determined using ELISA as previously described.[36] The wavelength of 450 nm was primarily used to determine the absorption values, but if the absorption values were too high (i.e. overflow was observed), the wavelength of 405 nm was used instead. Additionally, the skin tissues of the last injection sites were collected, fixed, sectioned, and then stained with hematoxylin and eosin (H&E) at the University of Texas MD Anderson Cancer Center Science Park Research Division (Smithville, TX) before examination.

Statistical Analysis

For all figures, the values shown are mean ± SD. Statistical significance was determined by two-tailed Student's t-test for two-group analysis or one-way ANOVA for multiple group comparisons.

Results and discussion

Synthesis of Al-nanosticks in bicontinuous RM

The synthesis of Al-nanosticks was carried out in an RM system that consisting H_2O, NP-5 and cyclohexane. The molar ratio of water to surfactant (i.e. NP-5), known as **ω**, in such ternary mixture system was ~16. This **ω** value was selected because it has been verified that bicontinuous RM with channel-like water phase forms when the **ω** value in such ternary system is greater than 10.[32–33] As shown in Figure 1A, the bicontinuous RM containing $AlCl_3$ or ammonium hydroxide was prepared separately. They were then mixed with each other to initiate the reaction between Al^{3+} and OH^-. After the nucleation stage, the resultant seed particles likely grew along the direction of water channels rather than the direction perpendicular to the outer surface of the wall of water channels due to the occupation of such surface by NP-5. As a result, the final products formed were thin stick-like nanoparticles as shown in Figure 1B. The length and diameter of the Al-nanosticks were about ~80 nm and ~8 nm, respectively, equaling an aspect ratio of ~10. Interestingly, the Al-nanosticks have much better monodispersity compared to the aggregated aluminum

hydroxide particles prepared by a ‘co-precipitation’ method (Figure S1) or to the less monodisperse particular aggregates consisting of AlOOH nanorods that were prepared by Sun et al. using a hydrothermal method.[13] It is likely that the surfactants at the interface of the water channel limit the attachment among different nanoparticles and thus the formation of large aggregates in the particle growth stage.

Characterization of the Al-nanosticks

Figure 2A shows the XRD analysis of the Al-nanosticks and three other types of aluminum (oxy)hydroxide, including the particles prepared by a ‘co-precipitation’ method,[35] the commercial Alhydrogel, and a commercial aluminum hydroxide (powder form). All four samples were subjected to lyophilization before characterization. The characteristic peaks of bayerite and boehmite (PDF No. 00–020-0011 and 00–021–1307, respectively, from the Joint Committee on Powder Diffraction Standards) are labeled for all samples. As shown in Figure 2A, the Al-nanosticks are mainly amorphous due to the huge characteristic peak in the 2θ range of 10–25. Moreover, their XRD pattern also contains the major characteristic peaks of boehmite and bayerite. For instance, the shoulder peak shown at 2θ value of 14 and the broad peaks with 2θ values of 28, 38, 49, 65 and 72 matched well with the boehmite standard. The small sharp peaks at 2θ values of 19, 41 and 53 and the shoulder peak at 2θ value of 21 agree with the bayerite standard, but not the gibbsite standard (details are shown in Figure S2). Compared to the Al-nanosticks, the major characteristic peaks in the XRD pattern of the commercial Alhydrogel agree well with that of the boehmite, suggesting that the Alhydrogel is mainly crystalline AlOOH, although the width of peaks indicates a moderate degree of crystallinity only. On the other hand, the XRD pattern of the aluminum hydroxide particles prepared by the ‘co-precipitation’ method contains multiple strong narrow peaks matching well with that of bayerite, as well as some weak peaks related to boehmite, demonstrating that this aluminate material is mainly composed of crystalline $Al(OH)_3$. Finally, the XRD pattern of the commercial aluminum hydroxide shows a broad peak in the 2θ range of 10–25, without any characteristic peak of any crystalline aluminate compounds, indicating that it is mainly amorphous $Al(OH)_3$.

Thereafter, TGA was carried out to further determine whether the Al-nanosticks are mainly amorphous $Al(OH)_3$ or amorphous AlOOH. Lugol’s solution was used to estimate the amount of residual NP-5 surfactant in the purified Al-nanostick preparation,[34] and the result showed that the residual NP-5 content was minimal (Figure S3). Figure 2B (red line) showed the TG curve of Al-nanosticks over the temperature range of 30 to 1000 °C and the relevant first derivative TG (DTG) curve was also plotted to distinguish the different stages of weight loss over such a temperature range. Besides the first stage of weight loss occurring below 150 °C related to the evaporation of water absorbed on the material surface,[37] the Al-nanosticks also have two additional stages of weight loss within the temperature range of 150 – 250 °C (~5.7%) and 250 – 450 °C (~10.8%). Moreover, because the DTG curve of the aluminum hydroxide particles prepared by the ‘co-precipitation’ method (composed of crystalline $Al(OH)_3$) has a large peak within 150 – 300 °C,[38] the weight loss occurring within the similar temperature range (i.e. 150 – 250 °C) from the Al-nanosticks may be attributed to the small portion of crystalline $Al(OH)_3$ formed during the synthesis (indicated by XRD pattern in Figure 2A). Furthermore, the TGA curve of the commercial aluminum

hydroxide (mainly composed of amorphous $Al(OH)_3$) shows a dramatic weight loss below 300 °C, which is significantly different from that of the Al-nanosticks, indicating that the main component of Al-nanosticks is not amorphous $Al(OH)_3$. On the other hand, the commercial Alhydrogel (composed of crystalline AlOOH) has a significant weight loss around 300 – 500 °C, which is probably related to the dehydroxylation of AlOOH.[39] Given that the dehydroxylation of materials with lower crystallinity tends to occur at a relatively lower temperature,[13] the DTG peak appearing in the slightly lower temperature range of 250 – 450 °C for the Al-nanosticks is more likely related to amorphous AlOOH.

To further confirm the main chemical composition of Al-nanosticks, XPS was used to characterize the aluminum samples, and the high-resolution XPS O 1s spectra are shown in Figure 2C. Each broad O 1s peak was deconvoluted into different contributions, and the peaks appearing around 530.5, 531.8 and 533.0 eV (pink, dark gray and yellow dashed lines in Figure 2C) can be attributed to the O atom of 'Al-O-Al' ($O_{Al\text{-}O\text{-}Al}$), 'Al-O-H' ($O_{Al\text{-}O\text{-}H}$), and 'H-O-H' (i.e. absorbed H_2O), respectively.[40–41] For our Al-nanosticks, the ratio of $O_{Al\text{-}O\text{-}Al}$ to the total amount of O in the structure ($O_{structure}$, i.e. $O_{Al\text{-}O\text{-}Al} + O_{Al\text{-}O\text{-}H}$) was calculated to be 34.2%, which is slightly lower than that of commercial Alhydrogel (39.2%), but much higher than that of the aluminum hydroxide particles prepared by the 'co-precipitation' method (19.9%) and commercial aluminum hydroxide (almost 0%). This indicates that our Al-nanosticks contain abundant 'Al-O-Al' structure units similar to the commercial Alhydrogel (known to be crystalline AlOOH as mentioned above). Since the 'Al-O-Al' structure unit cannot exist in pure aluminum hydroxide ($Al(OH)_3$) materials, the high $O_{Al\text{-}O\text{-}Al}/O_{structure}$ ratio of Al-nanosticks thus offers direct evidence that the main chemical component of such aluminum material is AlOOH.

In addition to the O 1s spectra, the high-resolution Al 2p spectra are shown in Figure 2D. The binding energy of Al atom in Al-nanosticks is 74.2 eV, which is slightly higher than that of commercial Alhydrogel (74.0 eV). This agrees with that higher content of hydroxyl groups resulting in higher binding energy of Al,[42] because Al-nanosticks (mainly amorphous AlOOH, with a small portion of crystalline $Al(OH)_3$ as shown in Figure 2A) have a higher amount of hydroxyl groups as compared to the Alhydrogel (moderately crystalline AlOOH). Similarly, the binding energy of Al atom in the commercial aluminum hydroxide (amorphous $Al(OH)_3$, 74.4 eV) is also slightly higher than that in the aluminum hydroxide particles prepared by the 'co-precipitation' method (mainly crystalline $Al(OH)_3$, with a small portion of poor crystalline AlOOH as shown in Figure 2A, 74.2 eV).

Taken together, the XRD, TGA, and XPS results confirmed that the Al-nanosticks are mainly amorphous AlOOH. Usually, the crystallinity of aluminum salt-based material synthesized in aqueous solution is predominately determined by the reaction temperature: room temperature mediates the formation of $Al(OH)_3$ (e.g. the aluminum hydroxide particles prepared by the 'co-precipitation' method), whereas high temperatures (e.g. over 90 °C) induce the generation of AlOOH.[13, 43] Interestingly, our Al-nanosticks, although formed at room temperature, are mainly composed of amorphous AlOOH. The underlying mechanism is unclear, but it is probably related to the polyoxyethylene moiety of the NP-5 surfactant that interacts strongly with H_2O molecules in the bicontinuous RM: in common aqueous solution, the formation of $Al(OH)_3$ (e.g. aluminum hydroxide particles prepared by 'co-

precipitation' method) is predominant (reaction (1)); in bicontinuous RM, sharply reducing the amount of free water molecules may primarily facilitate reaction (2), i.e. promoting the formation of AlOOH (e.g. Al-nanosticks).

$$Al^{3+} + 3OH^- \rightarrow Al(OH)_3 \quad (1)$$

$$Al^{3+} + 3OH^- \rightarrow AlOOH + H_2O \quad (2)$$

In conclusion, the bicontinuous RM-based synthesis method is able to modulate the physico-chemical properties of the resultant aluminum salt-based materials. The as-synthesized Al-nanosticks have a long aspect ratio and nanometer-scale size with reduced aggregation, likely because the unique channel-like water phase induces the growth of crystals and prevents the self-attachments. Importantly, such Al-nanosticks mainly consisting of AlOOH with low degree of crystallinity can form under a mild reaction condition (e.g. room temperature versus over ~90 °C), which may be attributed to the surfactants in the bicontinuous RM reducing the amount of free water molecules. Furthermore, the physico-chemical properties of the Al-nanosticks may improve their ability to potentiate immune responses, prompting us to evaluate their adjuvant activity using OVA as a model antigen.

Characterization of OVA-adsorbed Al-nanosticks

Figure 3A shows the binding isotherm of OVA to our Al-nanosticks. The weight ratio of Al^{3+}/OVA required for the full adsorption of OVA to the Al-nanosticks is about 0.1/1. Since the commercial Alhydrogel is chemically predominately AlOOH and has been selected as the International Standard Preparation of aluminum (oxy)hydroxide gels,[44–45] it was used as a control in all the following *in vitro* and *in vivo* studies. The TEM images of the Alhydrogel revealed that it is mainly composed of irregular aggregates of rod-like nanoparticles with overall size ranging from hundreds of nanometers to several microns (Figure S4). As expected, the weight ratio of Al^{3+}/OVA required for the full adsorption of OVA by the Alhydrogel is about 1/1 (Figure 3A), which is about 10-fold higher than that is required for the Al-nanosticks, likely because the Al-nanosticks with good monodispersity have a much larger available total surface area for OVA adsorption.[46]

The hydrodynamic size and zeta potential of the OVA-adsorbed Al-nanosticks or commercial Alhydrogel as a function of the weight ratios of Al^{3+}/OVA was determined by the dynamic light scattering (DLS) method. Although the DLS method may not accurately determine the hydrodynamic sizes of the non-spherical nanomaterials, it has been verified that the particle size data are reflective of the aggregation status of the AlOOH particles after binding to a protein antigen.[13] As shown in Figure 3B, the strongest aggregation of OVA-adsorbed Al-nanosticks or OVA-adsorbed commercial Alhydrogel was found when the weight ratio of the Al^{3+}/OVA was around 0.1/1 and 1/1, respectively, likely due to the neutralization of surface charges between the particles and OVA at those ratios (Figure 3C). Notably, when the Al^{3+}/OVA ratio was increased to 5/1, the hydrodynamic sizes of the OVA-adsorbed Al-nanosticks and the OVA-adsorbed commercial Alhydrogel are ~200 nm and

~1.2 μm, respectively, which are close to the sizes of the respective original particles without OVA adsorption (i.e. ~150 and ~900 nm), indicating that the OVA-adsorbed particles were well suspended (Figure 3B).

The zeta potentials of the resultant OVA-adsorbed Al-nanosticks and OVA-adsorbed commercial Alhydrogel prepared at the Al^{3+}/OVA ratio of 5/1 were similar (i.e. around ~20 mV as shown in Figure 3C). As a result, the OVA-adsorbed Al-nanosticks and the OVA-adsorbed commercial Alhydrogel prepared with the Al^{3+}/OVA ratio of 5/1 were selected for further immunization studies. Shown in Figure 3D is a representative TEM image of the OVA-absorbed Al-nanosticks. It appears that the OVA adsorption did not significantly change the overall structure of the Al-nanosticks.

Uptake of OVA adsorbed on the Al-nanosticks by J774A.1 macrophages

Because the adjuvant activity of aluminum salt-based materials is partially related to their ability to increase antigen uptake by APCs,[47–48] we tested whether the Al-nanosticks can effectively deliver OVA into APCs such as macrophages. Figure 4 shows the confocal microscopic image of J774.1A murine macrophages incubated with free FITC-labeled OVA (FITC-OVA) or FITC-OVA adsorbed on Al-nanosticks or Alhydrogel for six hours (Al^{3+}, 10 μg/mL; Al^{3+}/FITC-OVA weight ratio, 5/1). The intracellular green fluorescence signal is stronger in cells incubated with FITC-OVA adsorbed on the Al-nanosticks than in cells incubated with free FITC-OVA. However, for the FITC-OVA adsorbed on the Alhydrogel, it seems that the majority of the green fluorescence signals are extracellular, although associated or bound to the cell membrane (i.e. the location of green fluorescence is outside of the cell membrane indicated in red in the images). Therefore, it appears that more FITC-OVA adsorbed on the Al-nanosticks was internalized by the macrophages than that adsorbed on the Alhydrogel, likely related to the nanometer-scale size and unique stick-like shape of such Al-nanosticks.[16, 49–50]

IL-1β secretion by THP-1 cells after stimulation with Al-nanosticks

Thereafter, we evaluated the ability of the Al-nanosticks in activating inflammasomes. Human THP-1 monocytes were differentiated into macrophages, followed by treatment with Al-nanosticks or Alhydrogel in the presence or absence of LPS to stimulate IL-1β secretion. As shown in Figure 5, cells treated with the Al-nanosticks released significantly more IL-1β than those treated with the Alhydrogel. These results suggest that the Al-nanosticks are more effective than the Alhydrogel in activating inflammasomes. This may be partially attributed to the relatively low degree of crystallinity of the Al-nanosticks (Figure 2A).[13]

Potentiating OVA-specific immune responses by Al-nanosticks in vivo

To test the adjuvant activity of the Al-nanosticks, OVA-adsorbed Al-nanosticks (5 μg OVA with an Al^{3+}/OVA weight ratio of 5/1) were s.c. injected into mice every two weeks for a total of three times. Free OVA and OVA-adsorbed Alhydrogel were used as controls. Thirty-one days after the last injection, serum samples were collected to measure OVA-specific antibody levels. As shown in Figure 6, the OVA-adsorbed Al-nanosticks induced significantly higher levels of serum anti-OVA IgG and IgG1 than OVA-adsorbed Alhydrogel, demonstrating that the Al-nanosticks have stronger activity in potentiating humoral immune

response. This may be attributed, at least in part, to that the Al-nanosticks adsorb antigens more efficiently, increase the cellular uptake of antigens adsorbed on them by APCs, and activate inflammasomes more effectively (Figure 3–5). We only used OVA as a model antigen and fixed the ratio of Al^{3+} to OVA at 5/1 in the present study. More studies using different antigens and different Al^{3+} to antigen ratios will be needed to fully evaluate the adjuvant activity of our Al-nanosticks. In addition, neither the OVA-adsorbed Al-nanosticks nor the OVA-adsorbed Alhydrogel induced any significant anti-OVA IgG2a response (Figure 6C), indicating that an alternative modification of aluminum (oxy)hydroxide is needed to enable it to help antigens to induce specific IgG2a response (i.e. Th1 response).

Finally, we collected the skin samples at the last injection site for H&E staining. As expected, both Al-nanosticks and Alhydrogel induced local subcutaneous nodule and granuloma formulation, although the site injected with the Al-nanosticks has a relatively lower cellularity, especially in the center of the nodule, and less epidermal hyperplasia, as compared to the site injected with the Alhydrogel (Figure 7). Therefore, the local inflammatory reactions induced by the Al-nanosticks were not more severe than that induced by Alhydrogel.

Conclusions

In this work, for the first time, the bicontinuous RM technique was utilized to synthesize Al-nanosticks, a new aluminum salt-based material that are mainly composed of monodisperse amorphous AlOOH particles with nanometer-scale size (length of 80 nm) and stick-like shape (aspect ratio of ~10). Compared to the commercial Alhydrogel, such Al-nanosticks are more effective in adsorbing and delivering antigens (e.g. OVA) into antigen-presenting cells, activating inflammasomes, and enhancing antigen-specific immune responses in a mouse model. The aluminum (oxy)hydroxide nanosticks synthesized in bicontinuous RM have desirable physico-chemical properties and potent vaccine adjuvant activity.

Supplementary Material

Refer to Web version on PubMed Central for supplementary material.

Acknowledgments

This work was supported in part by the U.S. National Institutes of Health (AI105789 and CA135274 to Z.C.) and the Alfred and Dorothy Mannino Fellowship in Pharmacy at UT Austin (to Z.C.). Z.C. is also supported by the National Natural Science Foundation of China (81460454) and the Inner Mongolia Natural Science Fund (2014ZD05), S.A.V. is supported by the Becas-Chile Scholarship from the Government of Chile. S.H. is supported by a fellowship from the American Foundation for Pharmaceutical Education.

References

1. Koff WC, Burton DR, Johnson PR, Walker BD, King CR, Nabel GJ, Ahmed R, Bhan MK, Plotkin SA. Accelerating Next-Generation Vaccine Development for Global Disease Prevention. Science. 2013; 340:1232910. [PubMed: 23723240]
2. Zhu M, Wang R, Nie G. Applications of Nanomaterials as Vaccine Adjuvants. Hum. Vaccines Immunother. 2014; 10:2761–2774.
3. Grimm SK, Ackerman ME. Vaccine Design: Emerging Concepts and Renewed Optimism. Curr. Opin. Biotechnol. 2013; 24:1078–1088. [PubMed: 23474232]

4. He P, Zou Y, Hu Z. Advances in Aluminum Hydroxide-Based Adjuvant Research and Its Mechanism. Hum. Vaccines Immunother. 2015; 11:477–488.
5. Kuroda E, Coban C, Ishii KJ. Particulate Adjuvant and Innate Immunity: Past Achievements, Present Findings, and Future Prospects. Int. Rev. Immunol. 2013; 32:209–220. [PubMed: 23570316]
6. Kool M, Soullié T, van Nimwegen M, Willart MA, Muskens F, Jung S, Hoogsteden HC, Hammad H, Lambrecht BN. Alum Adjuvant Boosts Adaptive Immunity by Inducing Uric Acid and Activating Inflammatory Dendritic Cells. J. Exp. Med. 2008; 205:869–882. [PubMed: 18362170]
7. Exley C, Siesjö P, Eriksson H. The Immunobiology of Aluminium Adjuvants: How Do They Really Work. Trends Immunol. 2010; 31:103–109. [PubMed: 20153253]
8. Maughan CN, Preston SG, Williams GR. Particulate Inorganic Adjuvants: Recent Developments and Future Outlook. J. Pharm. Pharmacol. 2015; 67:426–449. [PubMed: 25496339]
9. Kool M, Fierens K, Lambrecht BN. Alum Adjuvant: Some of the Tricks of the Oldest Adjuvant. J. Med. Microbiol. 2012; 61:927–934. [PubMed: 22174375]
10. Marrack P, McKee AS, Munks MW. Towards an Understanding of the Adjuvant Action of Aluminium. Nat. Rev. Immunol. 2009; 9:287–293. [PubMed: 19247370]
11. O'Hagan DT, Fox CB. New Generation Adjuvants-from Empiricism to Rational Design. Vaccine. 2015; 33:B14–B20. [PubMed: 26022561]
12. Hem SL, HogenEsch H. Relationship between Physical and Chemical Properties of Aluminum-Containing Adjuvants and Immunopotentiation. Expert Rev. Vaccines. 2007; 6:685–698. [PubMed: 17931150]
13. Sun B, Ji Z, Liao Y-P, Wang M, Wang X, Dong J, Chang CH, Li R, Zhang H, Nel AE. Engineering an Effective Immune Adjuvant by Designed Control of Shape and Crystallinity of Aluminum Oxyhydroxide Nanoparticles. ACS Nano. 2013; 7:10834–10849. [PubMed: 24261790]
14. Li X, Aldayel AM, Cui Z. Aluminum Hydroxide Nanoparticles Show a Stronger Vaccine Adjuvant Activity Than Traditional Aluminum Hydroxide Microparticles. J. Controlled Release. 2014; 173:148–157.
15. Ruwona TB, Xu H, Li X, Taylor AN, Shi Y-c, Cui Z. Toward Understanding the Mechanism Underlying the Strong Adjuvant Activity of Aluminum Salt Nanoparticles. Vaccine. 2016; 34:3059–3067. [PubMed: 27155490]
16. Xu H, Li X, Cui Z. Toward Understanding the Mechanism Underlying the Strong Adjuvant Activity of Aluminum Salt Nanoparticles. Vaccine. 2017; 35:1102–1103. Ruwona Tb, Xu H, Li X, Taylor an, Shi Y, Cui Z. Vaccine 2016; 34: 3059-67. [PubMed: 28183431]
17. Wang T, Zhen Y, Ma X, Wei B, Wang N. Phospholipid Bilayer-Coated Aluminum Nanoparticles as an Effective Vaccine Adjuvant-Delivery System. ACS Appl. Mater. Interfaces. 2015; 7:6391–6396. [PubMed: 25780860]
18. Pileni M. Reverse Micelles as Microreactors. J. Phys. Chem. 1993; 97:6961–6973.
19. Capek I. Preparation of Metal Nanoparticles in Water-in-Oil (W/O) Microemulsions. Adv. Colloid Interface Sci. 2004; 110:49–74. [PubMed: 15142823]
20. Malik MA, Wani MY, Hashim MA. Microemulsion Method: A Novel Route to Synthesize Organic and Inorganic Nanomaterials: 1st Nano Update. Arabian J. Chem. 2012; 5:397–417.
21. Tovstun SA, Razumov VF. Preparation of Nanoparticles in Reverse Microemulsions. Russ. Chem. Rev. 2011; 80:953–969.
22. Eastoe J, Hollamby MJ, Hudson L. Recent Advances in Nanoparticle Synthesis with Reversed Micelles. Adv. Colloid Interface Sci. 2006; 128:5–15. [PubMed: 17254535]
23. Pileni M. Reverse Micelles Used as Templates: A New Understanding in Nanocrystal Growth. J. Exp. Nanosci. 2006; 1:13–27.
24. Acharya DP, Hartley PG. Progress in Microemulsion Characterization. Curr. Opin. Colloid Interface Sci. 2012; 17:274–280.
25. Pileni M-P. The Role of Soft Colloidal Templates in Controlling the Size and Shape of Inorganic Nanocrystals. Nat. Mater. 2003; 2:145–150. [PubMed: 12612669]
26. Tanori J, Pileni M. Control of the Shape of Copper Metallic Particles by Using a Colloidal System as Template. Langmuir. 1997; 13:639–646.

27. Xu S, Zhou H, Xu J, Li Y. Synthesis of Size-Tunable Silver Iodide Nanowires in Reverse Micelles. Langmuir. 2002; 18:10503–10504.
28. Rauscher F, Veit P, Sundmacher K. Analysis of a Technical-Grade W/O-Microemulsion and Its Application for the Precipitation of Calcium Carbonate Nanoparticles. Colloids Surf., A. 2005; 254:183–191.
29. Van der Zande BM, Böhmer MR, Fokkink LG, Schönenberger C. Aqueous Gold Sols of Rod-Shaped Particles. J. Phys. Chem. B. 1997; 101:852–854.
30. Wei K, Lai C, Wang Y. Formation of Monetite Nanoparticles and Nanofibers in Reverse Micelles. J. Mater. Sci. 2007; 42:5340–5346.
31. Li X, Naguib YW, Valdes S, Hufnagel S, Cui Z. Reverse Microemulsion-Based Synthesis of (Bis) Phosphonate-Metal Materials with Controllable Physical Properties: An Example Using Zoledronic Acid-Calcium Complexes. ACS Appl. Mater. Interfaces. 2017; 9:14478–14489. [PubMed: 28252282]
32. Chang C-L, Fogler HS. Controlled Formation of Silica Particles from Tetraethyl Orthosilicate in Nonionic Water-in-Oil Microemulsions. Langmuir. 1997; 13:3295–3307.
33. Bagwe RP, Yang C, Hilliard LR, Tan W. Optimization of Dye-Doped Silica Nanoparticles Prepared Using a Reverse Microemulsion Method. Langmuir. 2004; 20:8336–8342. [PubMed: 15350111]
34. Aldayel AM, Naguib YW, O'mary HL, Li X, Niu M, Ruwona TB, Cui Z. Acid-Sensitive Sheddable Pegylated Plga Nanoparticles Increase the Delivery of Tnf-[Alpha] SiRNA in Chronic Inflammation Sites. Mol. Ther.--Nucleic Acids. 2016; 5:e340. [PubMed: 27434685]
35. Patnaik, P., Dean, JA. Dean's Analytical Chemistry Handbook. 2. McGraw-Hill; New York: 2004.
36. Sloat BR, Sandoval MA, Hau AM, He Y, Cui Z. Strong Antibody Responses Induced by Protein Antigens Conjugated onto the Surface of Lecithin-Based Nanoparticles. J. Controlled Release. 2010; 141:93–100.
37. Wang J, Bokhimi X, Morales A, Novaro O, Lopez T, Gomez R. Aluminum Local Environment and Defects in the Crystalline Structure of Sol−Gel Alumina Catalyst. J. Phys. Chem. B. 1999; 103:299–303.
38. Du X, Wang Y, Su X, Li J. Influences of PH Value on the Microstructure and Phase Transformation of Aluminum Hydroxide. Powder Technol. 2009; 192:40–46.
39. Shen S, Ng WK, Chia LSO, Dong Y, Tan RBH. Morphology Controllable Synthesis of Nanostructured Boehmite and Γ-Alumina by Facile Dry Gel Conversion. Cryst. Growth Des. 2012; 12:4987–4994.
40. Kloprogge JT, Duong LV, Wood BJ, Frost RL. XPS Study of the Major Minerals in Bauxite: Gibbsite, Bayerite and (Pseudo-) Boehmite. J. Colloid Interface Sci. 2006; 296:572–576. [PubMed: 16236302]
41. Xu Z, Yu J, Low J, Jaroniec M. Microemulsion-Assisted Synthesis of Mesoporous Aluminum Oxyhydroxide Nanoflakes for Efficient Removal of Gaseous Formaldehyde. ACS Appl. Mater. Interfaces. 2014; 6:2111–2117. [PubMed: 24417734]
42. Kameshima Y, Yasumori A, Okada K. Xps and X-Ray AES (XAES) Study of Various Aluminate Compounds. Hyomen Kagaku. 2000; 21:481–487.
43. Naskar MK, Chatterjee M. Boehmite Nanoparticles by the Two-Reverse Emulsion Technique. J. Am. Ceram. Soc. 2005; 88:3322–3326.
44. Stewart-Tull, D. The Assessment and Use of Adjuvants. In: Gregory Gregoriadis, ACA., Poste, George, editors. Vaccines. Springer: New York; 1991. p. 85-92.
45. Oleszycka E, Lavelle EC. Immunomodulatory Properties of the Vaccine Adjuvant Alum. Curr. Opin. Immunol. 2014; 28:1–5. [PubMed: 24463269]
46. Cao, G. Nanostructures and Nanomaterials: Synthesis, Properties and Applications. World Scientific: London; 2004.
47. Foged C, Hansen J, Agger EM. License to Kill: Formulation Requirements for Optimal Priming of CD^{8+} CTL Responses with Particulate Vaccine Delivery Systems. Eur. J. Pharm. Sci. 2012; 45:482–491. [PubMed: 21888971]
48. Luo Z, Li P, Deng J, Gao N, Zhang Y, Pan H, Liu L, Wang C, Cai L, Ma Y. Cationic Polypeptide Micelle-Based Antigen Delivery System: A Simple and Robust Adjuvant to Improve Vaccine Efficacy. J. Controlled Release. 2013; 170:259–267.

49. Hutter E, Boridy S, Labrecque S, Lalancette-Hébert M, Kriz J, Winnik FM, Maysinger D. Microglial Response to Gold Nanoparticles. ACS Nano. 2010; 4:2595–2606. [PubMed: 20329742]

50. Niikura K, Matsunaga T, Suzuki T, Kobayashi S, Yamaguchi H, Orba Y, Kawaguchi A, Hasegawa H, Kajino K, Ninomiya T. Gold Nanoparticles as a Vaccine Platform: Influence of Size and Shape on Immunological Responses in Vitro and in Vivo. ACS Nano. 2013; 7:3926–3938. [PubMed: 23631767]

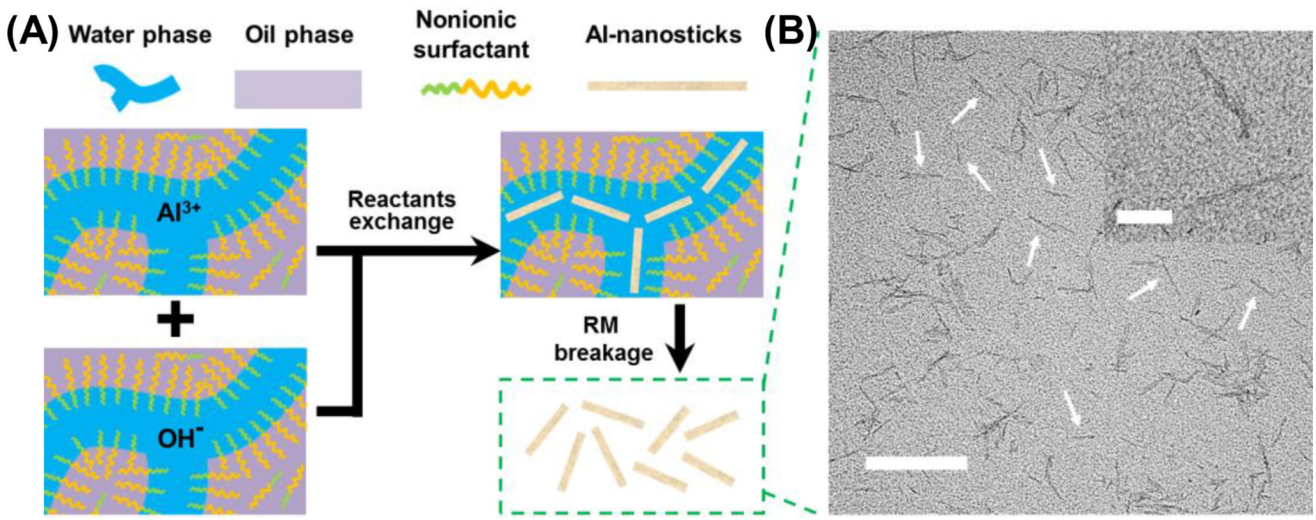

Figure 1.

(A) Schematic of the synthesis of the stick-like aluminum (oxy)hydroxide nanoparticles (Al-nanosticks) in a bicontinuous reverse microemulsion (RM). **(B)** A representative TEM image of the Al-nanosticks (bar = 200 nm). Monodisperse Al-nanosticks are indicated by white arrows (inset, an enlarged image of a nanostick, bar = 50 nm).

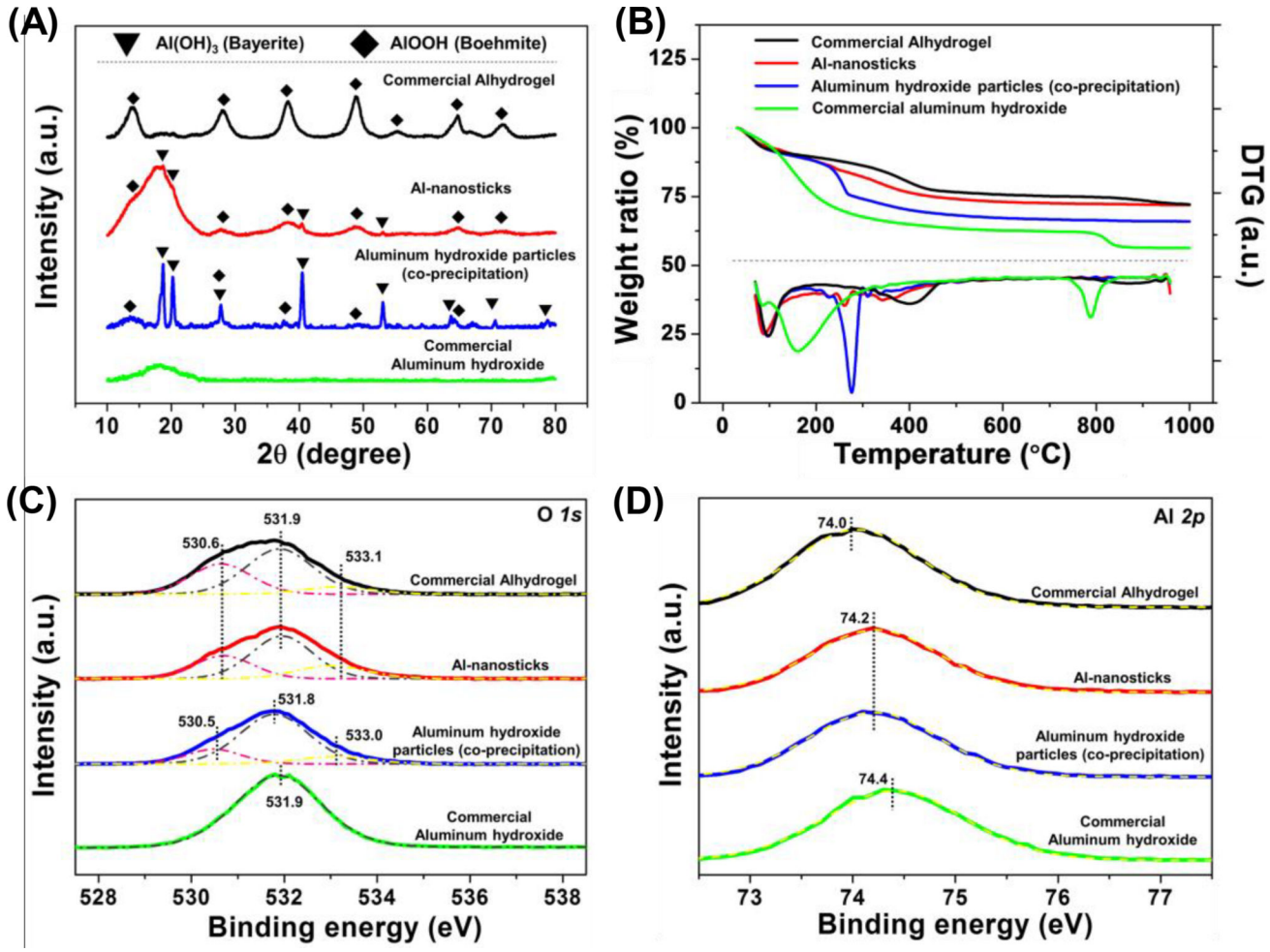

Figure 2.

Characterization of the Al-nanosticks. **(A)** XRD patterns to detect the crystallinity, in which the characteristic peaks of bayerite ($Al(OH)_3$, solid inverted triangle) and boehmite (AlOOH, solid rhombus) are labeled; **(B)** TGA and corresponding DTG analyses to investigate the dehydroxylation stages at different temperature ranges. **(C–D)** High resolution XPS spectra for the detection of atom ratios. (C) O 1s spectra, in which the raw data is deconvoluted into different contributions shown as pink, dark gray and yellow dashed lines; (D) Al 2p spectra, in which the fitting curve of raw data is shown as yellow dashed line. Commercial Alhydrogel, commercial aluminum hydroxide, and aluminum hydroxide particles prepared by a ‘co-precipitation’ method are included as controls.

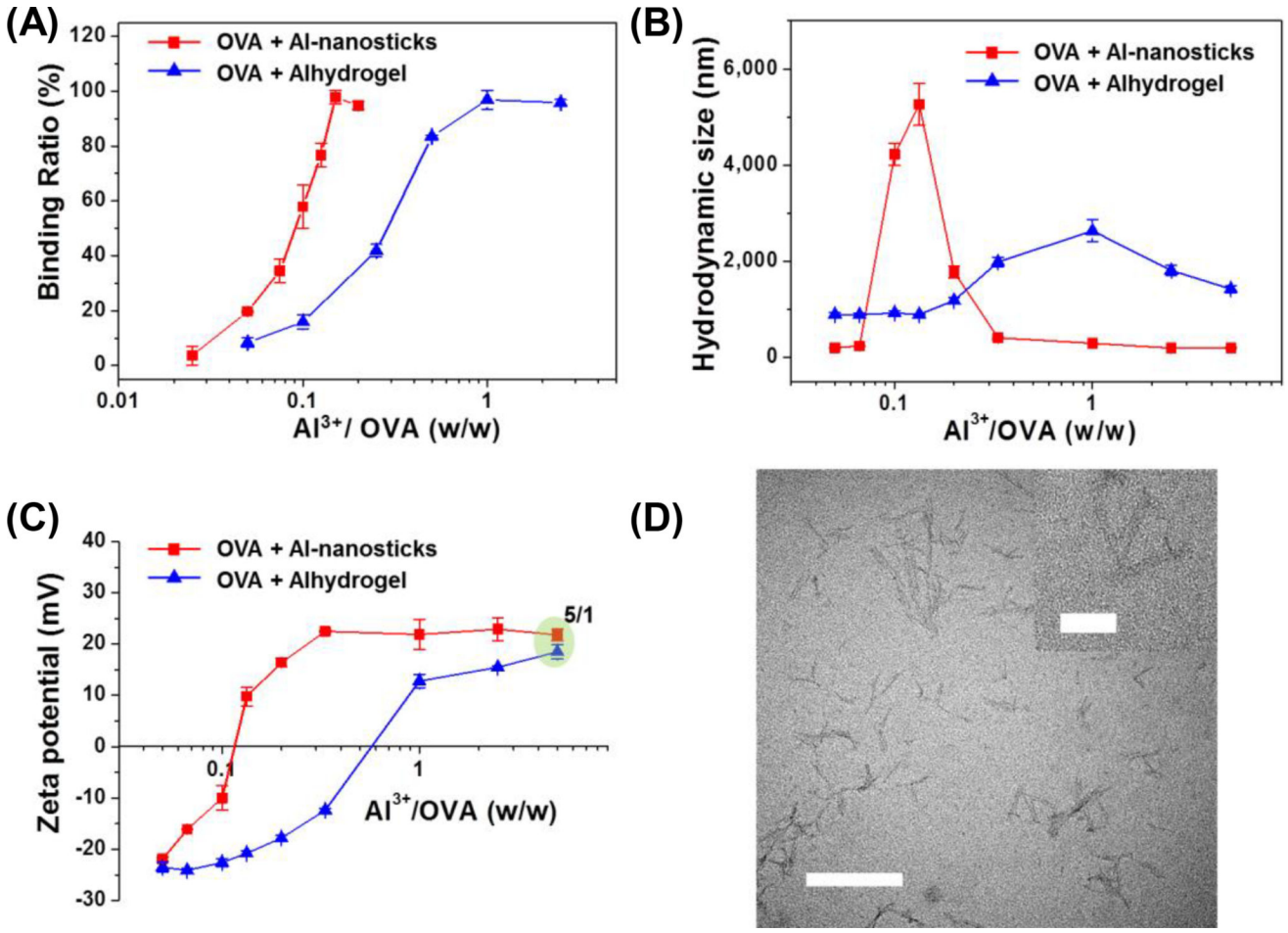

Figure 3.

Adsorption of OVA as a model antigen onto Al-nanosticks with the commercial Alhydrogel used as a control. **(A)** The binding isotherm of OVA to the Al-nanosticks; **(B–C)** the hydrodynamic sizes **(B)** and zeta potentials (**C**) of OVA-adsorbed Al-nanosticks as a function of the weight ratio of Al^{3+}/OVA in aqueous dispersions (n = 3). **(D)** A representative TEM image of OVA-adsorbed Al-nanosticks at an Al^{3+}/OVA weight ratio of 5/1 (bar = 200 nm). Inset is an enlarged image (bar = 50 nm).

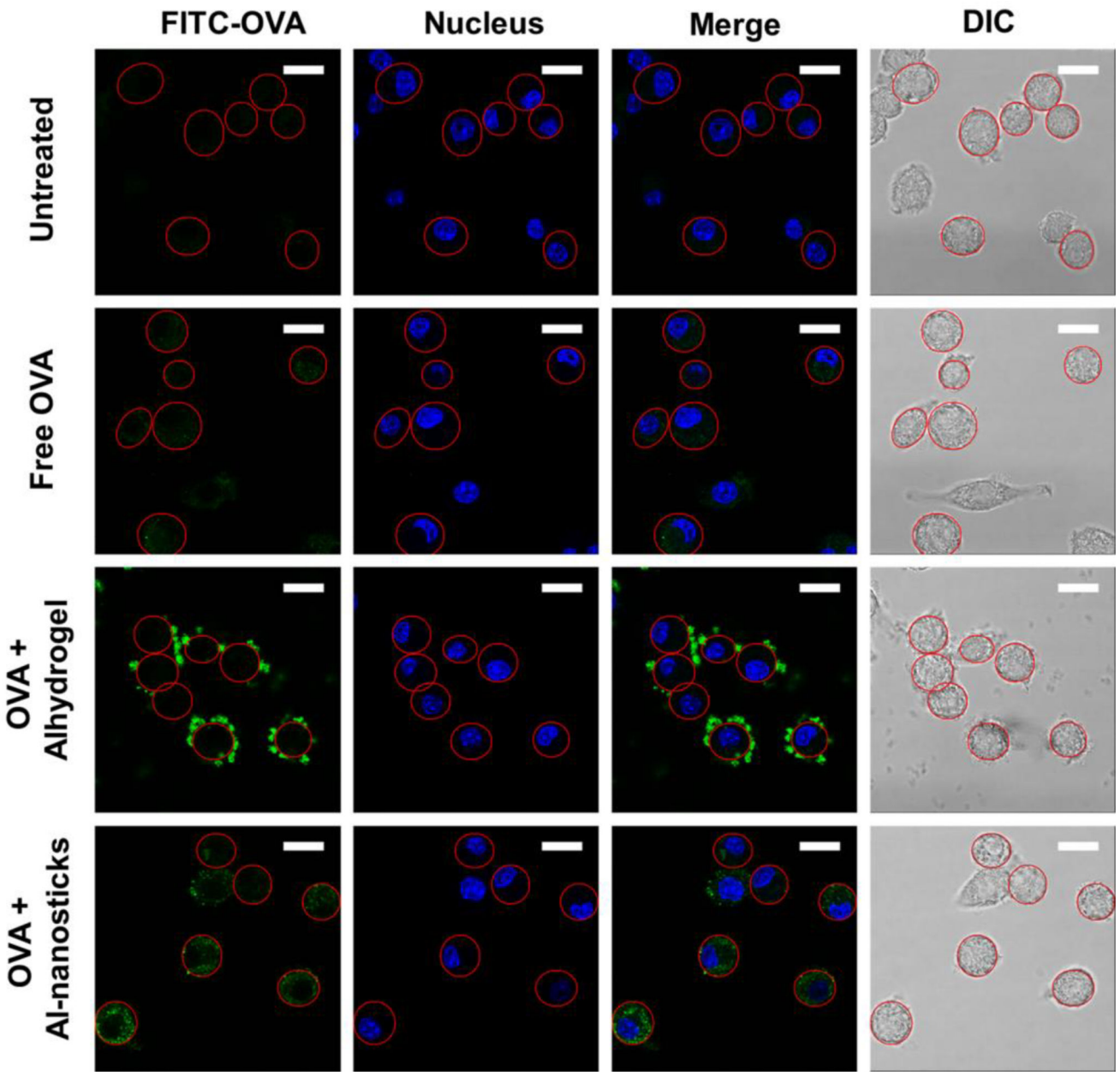

Figure 4.

Representative confocal microscopic images showing the uptake of FITC-labeled OVA (FITC-OVA) adsorbed on the Al-nanosticks by murine J774A.1 macrophages. Cells were incubated with FITC-OVA-adsorbed Al-nanosticks for 6 h (Al^{3+} of 10 μg/mL; Al^{3+}/FITC-OVA ratio of 5/1). As controls, cells were left untreated or treated with free FITC-OVA or FITC-OVA-adsorbed Alhydrogel at a fluorescence intensity equivalent to that of the FITC-OVA-adsorbed Al-nanosticks. Shown in green and blue represent FITC-OVA and DPAI-stained nucleus, respectively. The edge of some cells (or cell membrane) is indicated in red.

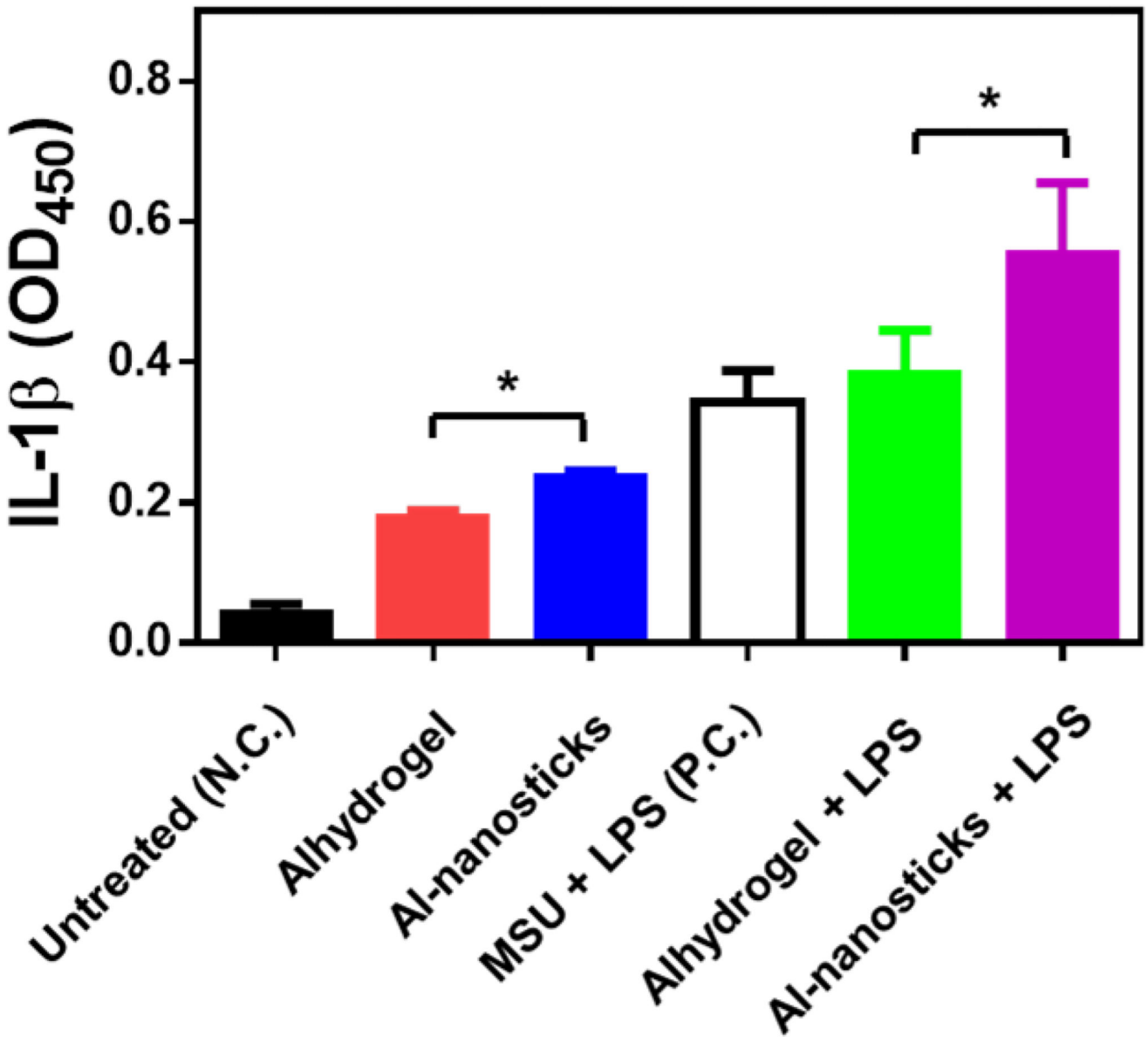

Figure 5.

IL-1β secretion by THP-1 cells induced by Al-nanosticks. Differentiated THP-1 cells were treated with Al-nanosticks or Alhydrogel (Al^{3+}, 50 μg/mL) in serum-free medium for 6 h at 37 °C and then stimulated with or without LPS (10 ng/mL) overnight before measuring IL-1β level in the culture medium using ELISA. Monosodium urate (MSU) crystal was a positive control. (n = 6; *, $p < 0.05$).

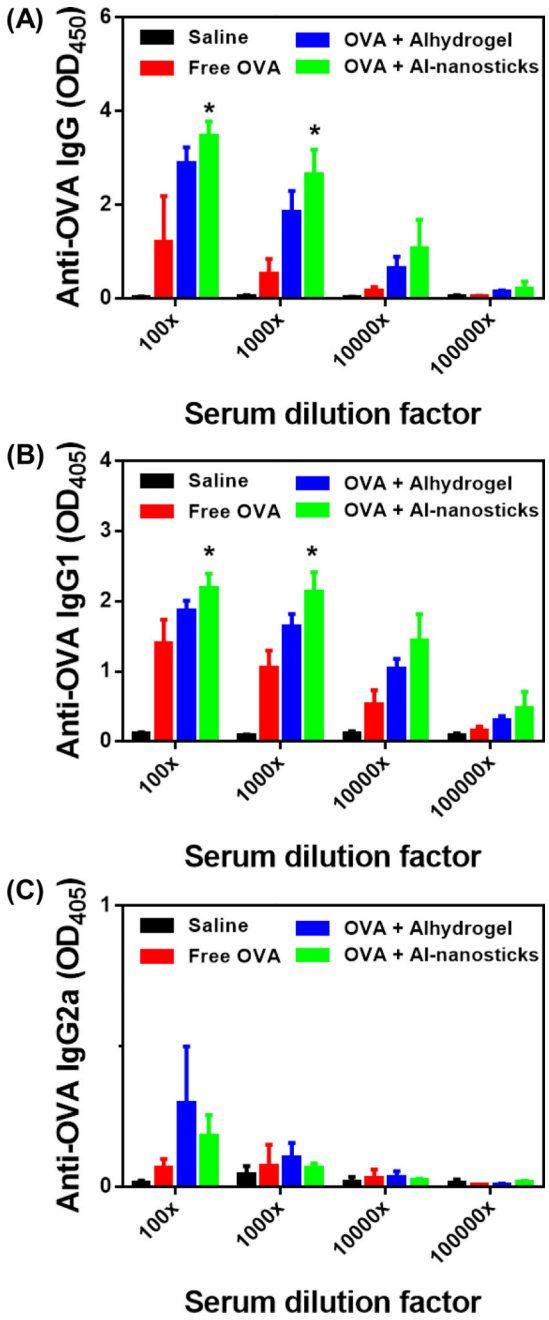

Figure 6.

OVA-specific total IgG and subtype levels in the serum samples of mice immunized with the OVA-adsorbed Al-nanosticks. BALB/c mice were s.c. injected with the OVA-adsorbed Al-nanosticks or commercial Alhydrogel on days 0, 15 and 30. Shown are total anti-OVA IgG **(A)**, IgG1 **(B)** and IgG2a **(C)** levels in mouse serum samples on day 61. (n = 5; *, $p < 0.05$, OVA+Al-nanosticks vs. OVA+Alhydrogel).

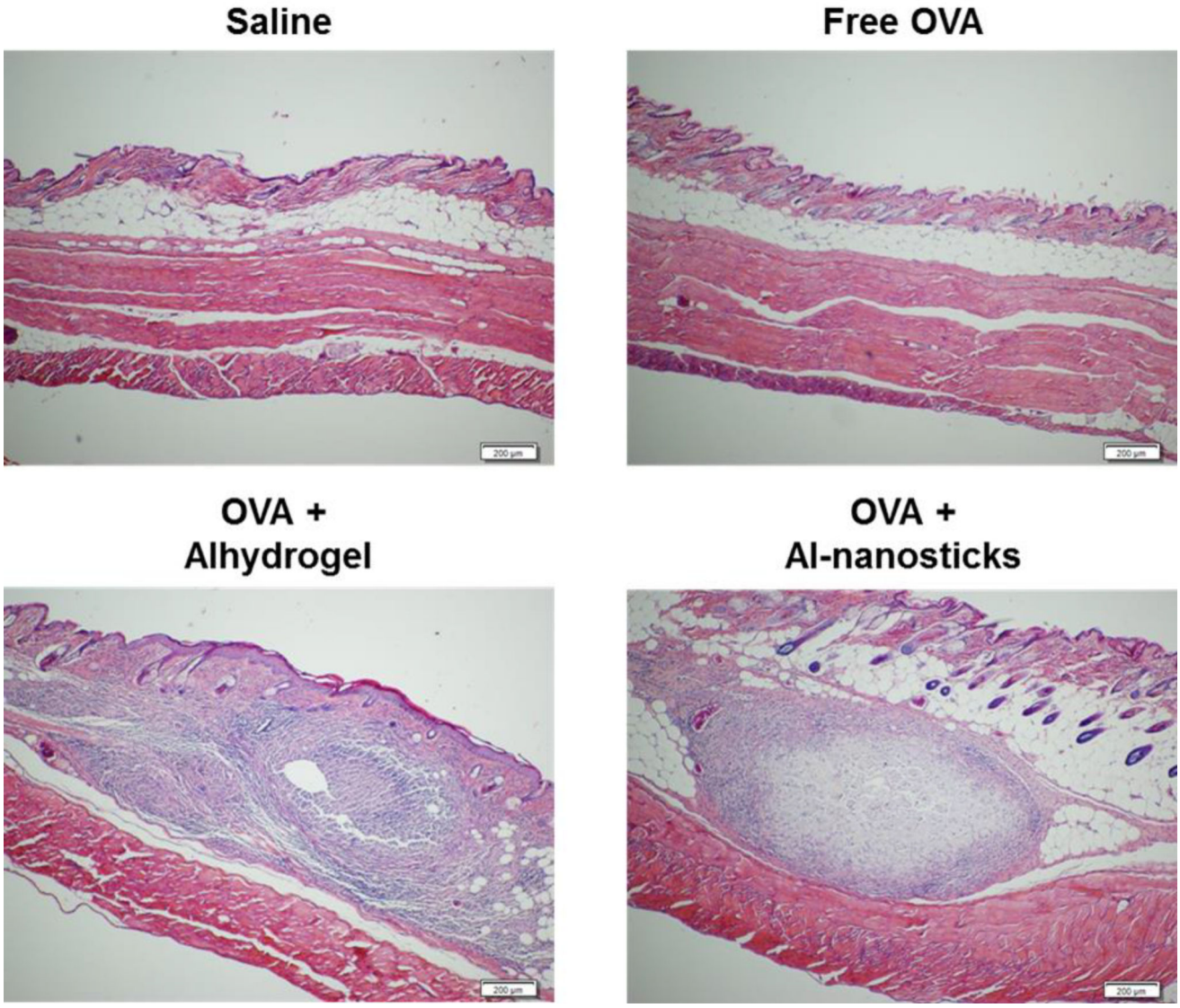

Figure 7.

Representative H&E histograms of mousee skin samples in the s.c. injection sites. Samples were taken from mice 31 days after injection with saline, free FITC-OVA, FITC-OVA-adsorbed Alhydrogel, or FITC-OVA-adsorbed Al-nanosticks (bar = 200 μm).